# Achieving Tunable Organic Afterglow and UV Irradiation-Responsive Ultralong Room-Temperature Phosphorescence from Pyridine-Substituted Triphenylamine Derivatives

*Shengde Xiong, Yu Xiong*, Deliang Wang, Yiwen Pan, Keyao Chen, Zheng Zhao, Dong Wang, and Ben Zhong Tang**

S. D. Xiong, Prof. Y. Xiong, Dr. D. L. Wang, Y. W. Pan, K. Y. Chen, Prof. D. Wang
Center for AIE Research, Shenzhen Key Laboratory of Polymer Science and Technology, Guangdong Research Center for Interfacial Engineering of Functional Materials, College of Materials Science and Engineering, Shenzhen University, Shenzhen 518061, China
E-mail: xiongyu@szu.edu.cn;

Prof. Z. Zhao, Prof. B. Z. Tang
School of Science and Engineering, Shenzhen Institute of Aggregate Science and Technology, The Chinese University of Hong Kong, Shenzhen, Guangdong 518172, China
E-mail: tangbenz@cuhk.edu.cn

Prof. Y. Xiong
HKUST Shenzhen Research Institute, Shenzhen 518057, China

**Keywords:** room-temperature phosphorescence, color-tunable, UV irradiation-responsive, phosphorescence energy transfer; anti-counterfeiting and information encryption

**Abstract:** Amorphous polymers with ultralong room-temperature phosphorescence (RTP) have received increasing attention for their various potential applications. However, multifunctional polymer-based RTP materials with multicolor afterglow or stimulus-responsiveness are highly desirable for multilevel anti-counterfeiting but rarely reported. Herein, we present a facile strategy to achieve a series of multifunctional polymer-based RTP materials with both color-tunable and UV irradiation-responsive characteristics by simply embedding pyridine-substituted triphenylamine derivatives into the poly(vinyl alcohol) (PVA) and poly(methyl methacrylate) (PMMA) matrices. Notably, introducing the pyridine groups with the capabilities of promoting intersystem crossing (ISC) and forming hydrogen-bonding networks is essential for triggering efficient and ultralong RTP from doping PVA systems, among which the doping film TPA-2Py@PVA exhibits excellent RTP property with an

ultralong lifetime of 798.4 ms and a high quantum yield of 15.2%. By further co-doping with the fluorescent dye rhodamine B, color-tunable persistent luminescence is realized via phosphorescence energy transfer. More importantly, doping PMMA systems exhibit reversible photo-activated ultralong RTP properties under continuous UV irradiation. Finally, diversified encryption patterns are devised to demonstrate potential applications of these doping PVA and PMMA systems in multilevel anti-counterfeiting and information encryption. We believe that multifunctional organic RTP materials with color-tunability and stimulus-responsiveness will provide new opportunities for high-tech applications.

## 1. Introduction

Organic RTP materials have attracted growing attention in the fields of anti-counterfeiting,[1] bioimaging,[2] sensing,[3] and optoelectronic devices[4] due to their unique advantages of long-lived triplet excitons and large Stokes shift. However, it is challenging to achieve efficient and persistent RTP emissions from metal-free organic phosphors due to their intrinsic spin-forbidden ISC and susceptibility of triplet excitons. To date, several strategies for improving RTP properties of pure organic systems have been proposed. On one hand, introducing carbonyl,[5] heteroatoms,[6] and halogens (Br and I)[7] can enhance spin-orbit coupling (SOC) to populate triplet excitons; On the other hand, crystallization engineering,[8] H-aggregation,[9] embedding organic phosphors into rigid polymer matrices,[10] supramolecular assembly,[11] and building 3D networks[12] can effectively suppress nonradiative deactivation pathways. Despite excellent RTP properties achieved for crystal-based organic small molecules,[13] amorphous organic RTP polymers stand out as a consequence of their advantages of good flexibility, processability, and machinability.[14] Therefore, it is highly desirable to develop efficient and ultralong polymer-based RTP materials.

In the past few years, various polymer-based RTP materials have been successfully developed through the methods of ring-opening polymerization,[2a] free-radical homopolymerization and copolymerization,[15] embedding organic phosphors into rigid polymer matrices, [10,16] and so on.[17] These methods focus on creating a rigid microenvironment or introducing noncovalent interactions between organic phosphors and polymer matrices to suppress nonradiative relaxations as much as possible, thus giving rise to efficient and long-lived RTP emissions. However, to realize advanced technological applications involving multi-dimensional signals, it is essential to develop multifunctional polymer-based RTP materials. Until recently, exploring smart polymer-based RTP materials with dynamic responses to external stimuli such as excitation wavelength, UV irradiation,

temperature, humidity, and mechanical force have been emerged as a hot topic.[18] For instance, An and co-workers observed color-tunable RTP emissions from a series of amorphous ionic polymers by changing the excitation wavelength.[19] Li's group presented a feasible strategy to achieve excitation-dependent multicolor RTP through covalently doping diversified arylboronic acids into the PVA matrix.[20] Apart from relying on the excitation wavelength, Ma et al. successfully realized color-tunable RTP emissions by utilizing a thermoreversible Diels-Alder reaction to construct dynamic covalent bonds.[21] To circumvent tricky molecular engineering, Kuila and George afforded an alternative strategy to achieve color-tunable persistent luminescence via phosphorescence energy transfer from long-lived organic phosphors (donors) to commercially available fluorescent dyes (acceptors).[22] By integrating multi-resonance fluorescent chromophores and organic phosphors with ultralong RTP emissions into a single-component copolymer, Chen and co-workers successfully obtained bright multicolor hyperafterglow.[15b] On the other hand, Ma et al. reported a series of novel carbonyl derivatives which exhibit photo-responsive RTP properties after being doped into the PMMA matrix.[23] Meanwhile, Yang et al. observed photo-responsive ultralong RTP emissions from doping PVA systems by constructing 3D covalent networks under continuous UV irradiation, [24] whereas Xu et al. prepared epoxy polymer containing 3D covalent networks as a new type of rigid matrix to induce switchable ultralong RTP emissions under UV irradiation.[12a] Besides, metal-free organic systems possessing protonation/force/photothermal-induced RTP properties have also been reported.[25] Despite these significant achievements, developing multifunctional polymer-based RTP materials with simultaneous multiple stimulus-responsiveness and color-tunability remains a formidable challenge.

Previously, we had been devoted to gaining some deeper insights into the emission mechanism of polymer-based RTP systems and achieving color-tunable organic afterglow for advanced anti-counterfeiting and information encryption applications.[16b,26] Herein, we further developed a series of polymer-based RTP systems with tunable organic afterglow and UV irradiation-responsive ultralong RTP characteristics for multilevel advanced anti-counterfeiting and information encryption applications. As illustrated in **Figure 1**, three triphenylamine (TPA) derivatives containing different numbers of pyridine groups were designed as guest phosphors for the following considerations: i) the electron-withdrawing pyridine group can not only reduce the energy gap between the singlet and triplet excited states ($\Delta E_{ST}$) but also promote the SOC, thus allowing for the enhancement of ISC efficiency; ii) the pyridine group can also form hydrogen-bonding (H-bonding) interactions with the PVA

matrix, which is favorable for the stabilization of triplet excitons; iii) the TPA skeleton is selected because of its twisted conformation which is beneficial to promote the SOC and avoid aggregation-caused quenching as well; iv) the number of pyridine group is regulated for improving RTP property by controlling the balance between the radiative decay rate of triplet excitons and H-bonding interactions between the pyridine group and PVA matrix. Excitedly, ultralong RTP emissions were successfully achieved by simply doping these pyridine-substituted TPA derivatives into the PVA matrix and multicolor organic afterglows were further realized through a facile strategy of phosphorescence energy transfer. More importantly, photo-activated ultralong RTP emissions with reversible response to the continuous UV irradiation (365 nm) were obtained by embedding these pyridine-substituted TPA derivatives into the rigid PMMA matrix. Besides, various encryption patterns were designed to demonstrate the potential applications of these pyridine-substituted TPA derivatives with ultralong lifetime, tunable persistent luminescence, and UV irradiation-responsiveness in multilevel anti-counterfeiting and information encryption technologies.

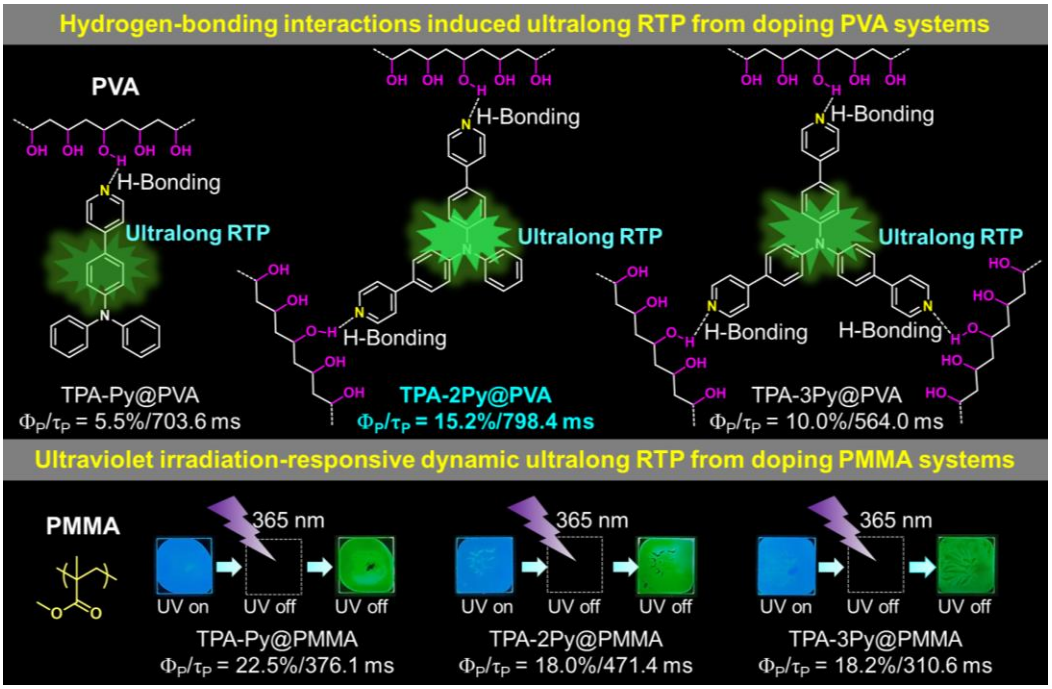


**Figure 1.** The chemical structures of guest phosphors TPA-Py, TPA-2Py, and TPA-3Py, and their RTP properties after being doped into the PVA and PMMA matrices.

## 2. Results and Discussion

As illustrated in **Figure 1**, the TPA skeleton bearing different numbers of pyridine groups, namely mono-pyridine substituted TPA (TPA-Py), di-pyridine substituted TPA (TPA-2Py), and tri-pyridine substituted TPA (TPA-3Py) were synthesized and further embedded as guest phosphors into the rigid PVA and PMMA matrices, respectively. All the doping PVA and

PMMA films were prepared by the drop-casting method which is simple and fast for the formation of thin solid films on small surfaces. Thermal annealing treatments were conducted to remove water or dimethyl formamide (DMF) residues after dropping a small amount of aqueous or DMF solutions containing both guest luminophore and polymer matrix onto the preheated quartz substrate. The optimal doping concentration of guest phosphors was determined to be 1.4 wt.% by adding 1.0 mg guest molecules into different amounts of aqueous (PVA, 30 mg $mL^{-1}$) or DMF solutions (PMMA, 30 mg $mL^{-1}$) (**Figure S1**). It should be noted that these pyridine-substituted TPA derivatives can form different degrees of H-bonding interactions with the PVA matrix, thus giving rise to a significant influence on their RTP properties after being doped into the PVA matrix.

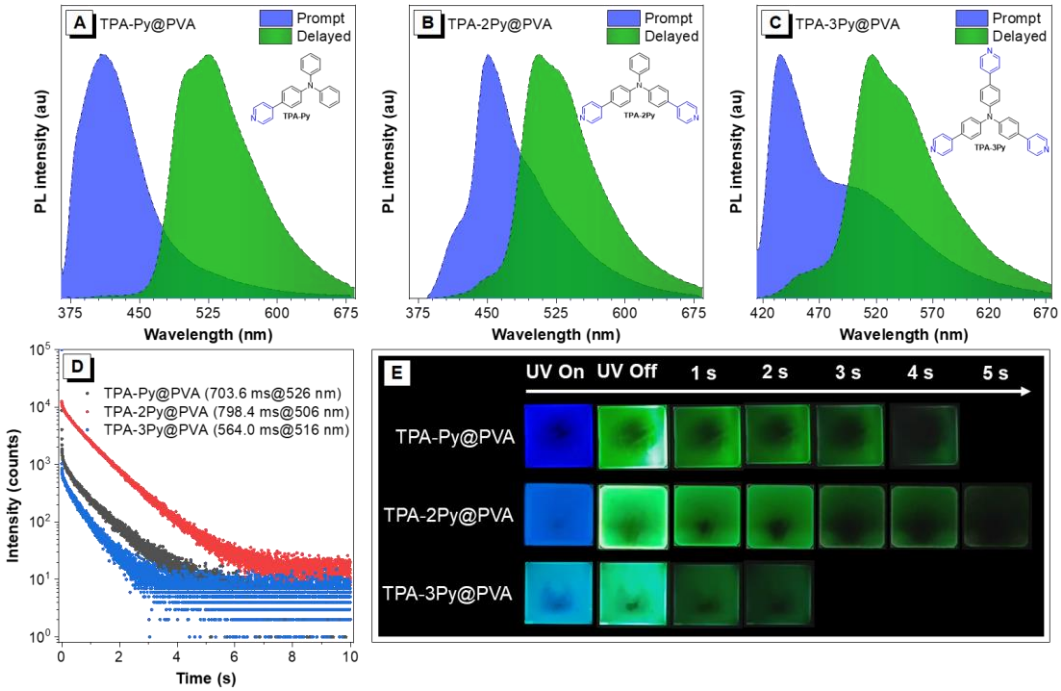


**Figure 2.** Photophysical properties of doping PVA films TPA-Py@PVA, TPA-2Py@PVA, and TPA-3Py@PVA: (A-C) prompt and delayed PL spectra; (D) time-resolved phosphorescent decay curves; (E) luminescence photographs under and after removing the UV irradiation (365 nm) with different duration times.

Although these pyridine-substituted TPA derivatives show no phosphorescence signal in dilute solutions or solid powders at ambient conditions, bright green afterglows lasting for seconds can be observed by the naked eye by doping them into the PVA matrix (**Figure 2E and Videos 1-3**). As shown in **Figure 2A-C**, the delayed emissions of doping PVA films TPA-Py@PVA, TPA-2Py@PVA, and TPA-3Py@PVA are redshifted remarkably relative to their corresponding prompt fluorescence. By fitting the time-resolved decay curves of prompt fluorescence and delayed emission, nanoseconds lifetimes of 2.09, 1.91, 1.24 ns and hundreds

of milliseconds of 703.6, 798.4, 564.0 ms are estimated for doping PVA films TPA-Py@PVA, TPA-2Py@PVA, and TPA-3Py@PVA respectively (**Figure 2D and Figure S2A**). These results show that these pyridine-substituted TPA derivatives possess dual-emission of prompt fluorescence and ultralong phosphorescence after being immobilized into the PVA matrix. On account of abundant hydroxyl groups on the PVA chain, the pyridine groups which are capable of forming H-bonding interactions with these hydroxyl groups are essential to inducing efficient and ultralong RTP emissions from these doping PVA systems. In particular, the doping film TPA-2Py@PVA exhibits the best RTP property with an ultralong lifetime of 798.4 ms and a high phosphorescence quantum yield of 15.2%, which might be attributed to an optimal balance between the radiative decay rate of triplet excitons and H-bonding interactions between the pyridine group and PVA matrix (**Figure S3**).

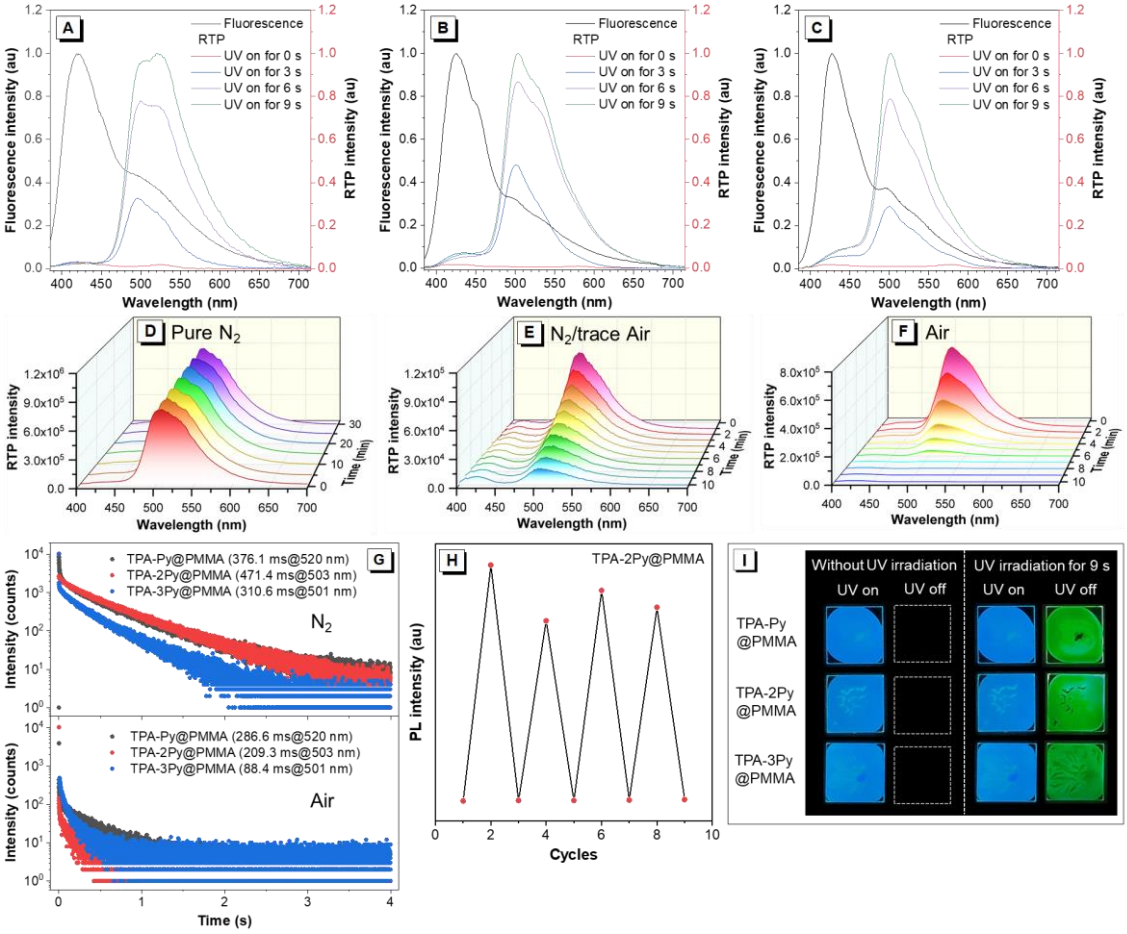


**Figure 3.** Photophysical properties of doping PMMA films TPA-Py@PMMA, TPA-2Py@PMMA, and TPA-3Py@PMMA: (A-C) the prompt fluorescence and photo-activated RTP emission spectra; (D-F) the fading process of photo-activated RTP emission of doping film TPA-2Py in pure $N_2$, $N_2$/trace air and air atmosphere, respectively; (G) time-resolved RTP decay curves measured in air and pure $N_2$ atmosphere, respectively; (H) phosphorescence intensity changes for the doping film TPA-2Py@PMMA during the UV

irradiation/recover cycles; (F) luminescence photographs under and after removing the UV irradiation (365 nm) with different duration times.

**Table 1.** Photophysical properties of doping PVA and PMMA films at room temperature. [a)]

| Doping PVA films | $\lambda_F$ [nm] | $\lambda_P$ [nm] | $\tau_F$[ns] | $\Phi_F$[%] | $\tau_P$[ms] | $\Phi_P$ [%] | $k_P$[$s^{-1}$] | $k_{NR}$[$s^{-1}$] | $k_{ISC}$[$s^{-1}$] |
|---|---|---|---|---|---|---|---|---|---|
| TPA-Py@PVA | 410 | 526 | 2.09 | 26.0 | 703.6 | 5.5 | $7.8\times10^{-2}$ | 1.34 | $2.6\times10^{7}$ |
| TPA-2Py@PVA | 450 | 506 | 1.91 | 22.1 | 798.4 | 15.2 | 0.19 | 1.06 | $8.0\times10^{7}$ |
| TPA-3Py@PVA | 435 | 516 | 1.24 | 13.8 | 564.0 | 10.0 | 0.18 | 1.59 | $8.1\times10^{7}$ |
| TPA-Py@PMMA | 420 | 520 | 2.25 | 44.8 | 286.6 (376.1) | 22.5 | 0.78 | 2.70 | $1.0\times10^{8}$ |
| TPA-2Py@PMMA | 425 | 503 | 1.42 | 38.5 | 209.3 (471.4) | 18.0 | 0.86 | 3.92 | $1.3\times10^{8}$ |
| TPA-3Py@PMMA | 427 | 501 | 1.43 | 40.1 | 88.4 (310.6) | 18.2 | 2.0 | 9.25 | $1.3\times10^{8}$ |

a) $\lambda_F$: fluorescence maximum; $\lambda_P$: phosphorescence maximum; $\tau_F$: fluorescence lifetime; $\Phi_F$: total quantum yield; $\tau_P$: phosphorescence lifetime; $\Phi_P$: phosphorescence quantum yield; $k_P$: radiative decay rate of phosphorescence; $k_{NR}$: nonradiative decay rate of phosphorescence; $k_{ISC}$: intersystem crossing rate; $k_P = \Phi_P/\tau_P$, $k_{NR} = (1 - \Phi_P)/\tau_P$, and $k_{ISC} = \Phi_P/\tau_F$; the lifetimes of doping PMMA films measured in nitrogen atmosphere are listed in brackets.

To further reveal the RTP emission mechanism of doping PVA systems, these pyridine-substituted TPA derivatives were embedded into the rigid PMMA matrix without the capability to form H-bonding interactions with pyridine groups. As expected, all the doping PMMA films exhibit no phosphorescence at ambient conditions. Only after exposure to continuous UV irradiation (365 nm) for about 9 seconds, bright green afterglows can be observed by the naked eye (**Figure 3** and **Videos 4-6**). As shown in **Figure 3A-C**, with increasing the UV irradiation time, the delayed emission of all the doping PMMA films appears and rapidly enhances to a saturation value within 9 seconds, indicating their photo-activated RTP properties. Particularly, the photo-activated RTP emissions of these doping PMMA films will be quenched within 5 min after exposure to the air but can be reactivated by continuous UV irradiation. Compared with the works reported in the literature, these doping PMMA systems show much faster response time.[12a,24,27] Considering that PMMA films have a poor oxygen barrier effect, the fading processes of UV irradiation-responsive RTP emissions were tested in pure nitrogen, nitrogen/trace air, and air atmospheres respectively to reveal the photo-activation mechanism. Due to the similar photo-activated RTP properties of all the doping PMMA films, the doping film TPA-2Py@PMMA was selected as a case study. As shown in **Figure 3D-F**, the photo-activated RTP emissions show no obvious decay after storing in pure nitrogen for 30 min. However, after introducing trace amounts of air into pure nitrogen, the decaying process of photo-activated RTP emission is triggered and is fully

quenched within 10 min. If pure nitrogen is further turned into air, the quenching process of photo-activated RTP emission is remarkably accelerated. These results indicate the significant influence of oxygen in air on the photo-activated RTP emissions of doping PMMA films. According to the reports in the literature, triplet photosensitizer can react with molecular oxygen ($^3O_2$) under photoexcitation to produce singlet oxygen ($^1O_2$) via the triplet-triplet energy transfer process.[28] Accordingly, we speculate that the diffusion of $^3O_2$ into the PMMA film could deactivate triplet excitons generated in guest phosphors, thus leading to undetectable RTP in the initial state. After a period of UV irradiation, the residual $^3O_2$ in PMMA film is converted into $^1O_2$, thus activating ultralong RTP emissions. To further verify the mechanism of UV irradiation-responsive RTP, the EPR (Electron Paramagnetic Resonance) spectra were measured to detect $^1O_2$ generated before and after continuous UV irradiation.[34] Indeed, the strong EPR signal of $^1O_2$ is observed only after exposure to continuous UV irradiation in an air atmosphere, indicating the conversion of $^3O_2$ into $^1O_2$. In addition, the lifetimes of photo-activated RTP emissions in the nitrogen are determined to be 376.1, 471.4, and 310.6 ms for TPA-Py@PMMA, TPA-2Py@PMMA, and TPA-3Py@PMMA respectively, which are much longer than those measured in an air atmosphere (**Figure 3G-H**). Besides, the switching between the activation and quenching of ultralong RTP emissions from these doping PMMA systems can be repeated for up to ten cycles (**Figure S6**).

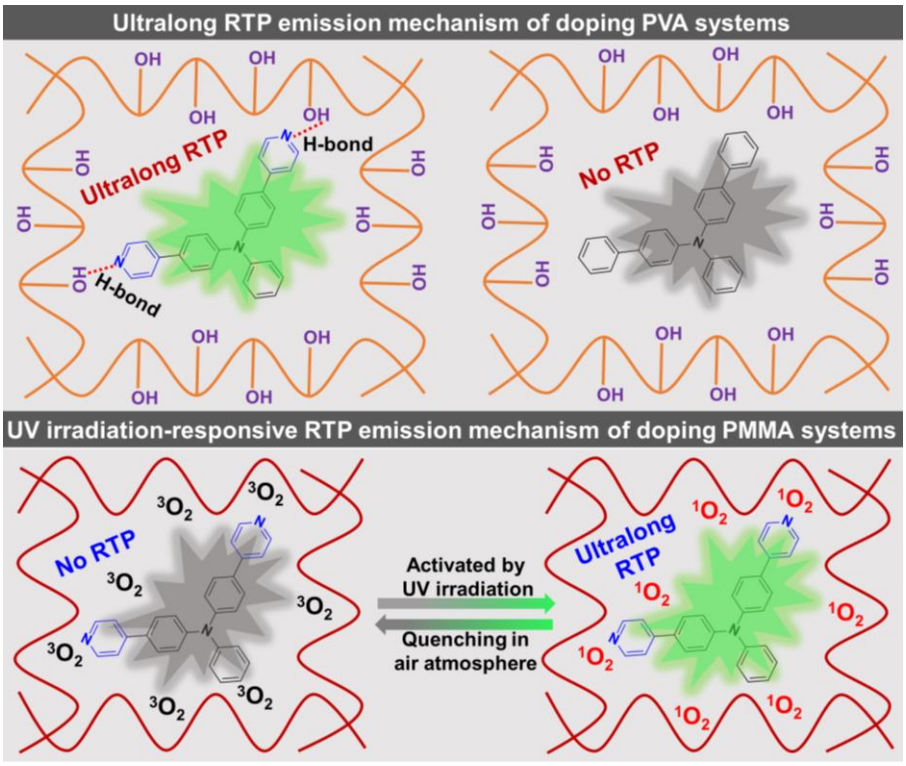

**Figure 4.** Illustration of different RTP emission mechanisms of pyridine-substituted TPA derivatives after being doped into the PVA and PMMA matrices.

To further reveal distinct emission mechanisms of these pyridine-substituted TPA derivatives doped into the PVA and PMMA matrices, we need to confirm the attribute of their ultralong RTP emissions. Primarily, all the pyridine-substituted TPA derivatives dissolved in dilute solutions display ultralong phosphorescence with lifetimes ranging from 0.75 to 1.30 s under cryogenic conditions (**Figure S10-11**), indicating their excellent single-molecular phosphorescence properties. Additionally, all the guest phosphors have good dispersion in PVA and PMMA matrices due to the ultralow doping concentration, thus leading to good overlap between the ultralong RTP emissions of doping polymer films and the low-temperature phosphorescence emissions of corresponding guest phosphors dissolved in dilute solutions. These results show that the ultralong RTP properties of both doping PVA and PMMA systems could be attributed to the inherent ultralong single-molecular phosphorescence of guest phosphors. This is because like the cryogenic effect, either creating a rigid microenvironment or introducing noncovalent interactions between guest phosphors and polymer matrix can effectively suppress nonradiative relaxations, thus achieving efficient RTP emission. Compared with the PMMA matrix without active hydroxy groups, all the pyridine-substituted TPA derivatives doped into the PVA matrix show excellent RTP properties without UV irradiation activation. Meanwhile, after changing the pyridine groups into phenyl groups, the reference compound (**TPA-2Ph**) with intrinsic ultralong low-temperature phosphorescence shows no RTP after being doped into the PVA matrix (**Figure 12-S13A**). These results demonstrate the crucial contribution of H-bonding interactions between the pyridine groups and the PVA matrix to the achievement of ultralong RTP properties of doping PVA systems. Besides, bright and persistent RTP from reference compound **TPA-2Ph** embedded in the PMMA matrix can also be activated by continuous UV irradiation (**S13B-C**), confirming that the silent RTP in the initial state is caused by the diffusion of $^3O_2$ into the PMMA film which could quench triplet excitons generated in guest phosphors. Therefore, the different RTP emission mechanisms of doping PVA and PMMA systems in the current study can be described as follows (**Figure 4**): i) the ultralong RTP emissions of doping PVA systems are induced by the intermolecular H-bonding interactions between the pyridine groups and abundant hydroxyl groups on the PVA chain; ii) the consumption of $^3O_2$ diffused into the PMMA matrix under continuous UV irradiation should be responsible for the UV irradiation-responsive ultralong RTP emissions of doping PMMA

systems. Notably, due to the refill of $^3O_2$ into the PMMA matrix, the photo-activated RTP will be fully quenched within 5 min after exposure to the air.

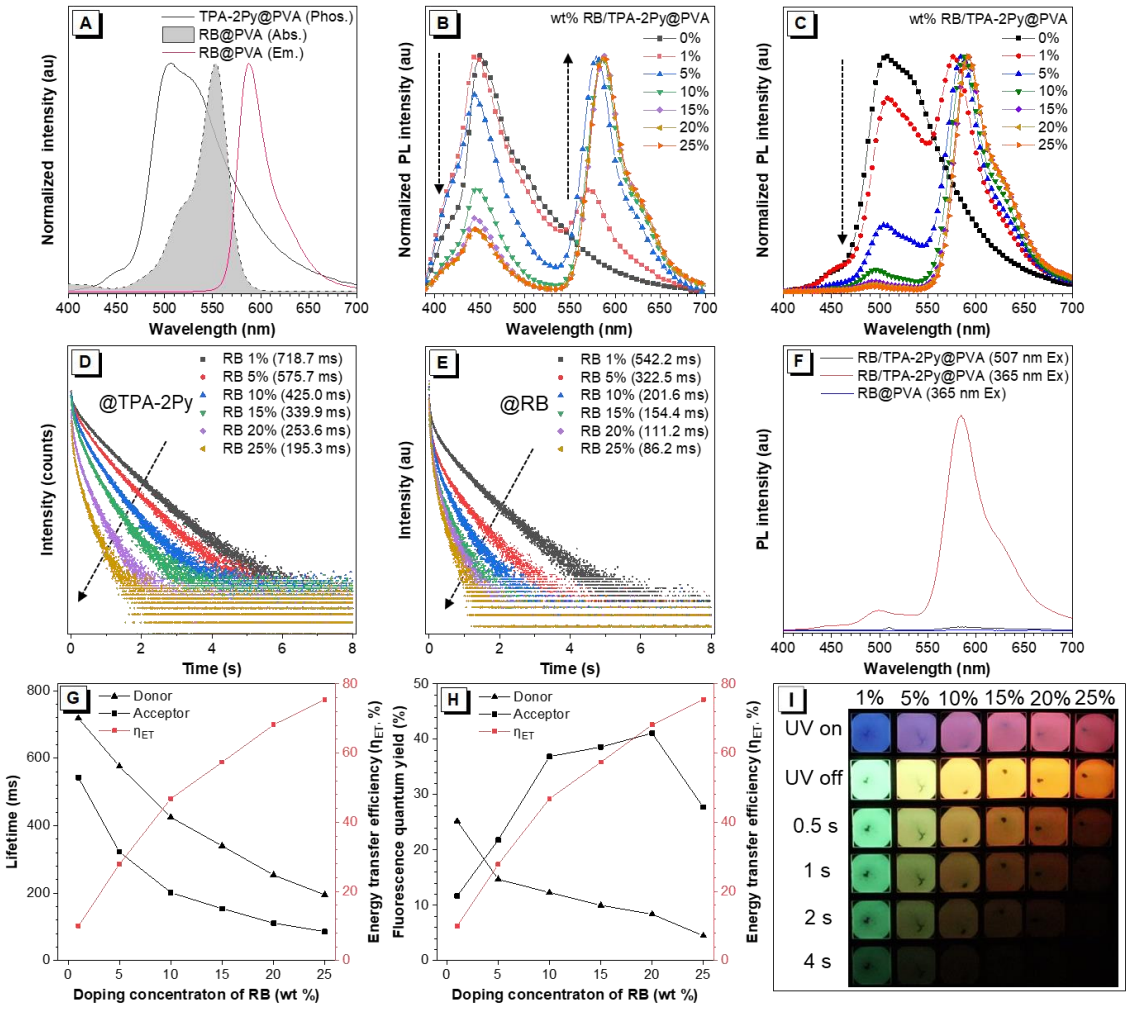


**Figure 5.** (A) Overlapped absorbance and fluorescence emission of doping film RB@PVA and phosphorescence emission of doping film TPA-2Py@PVA; (B-C) doping concentration-dependent prompt and delayed PL spectra of RB-codoped film TPA-2Py@PVA, respectively; (D-E) time-resolved delayed PL decay curves of RB-codoped film TPA-2Py@PVA; (F) excitation-dependent delayed emission spectra of 10%RB-codoped film TPA-2Py@PVA and doping film 10%RB@PVA; (G) the relationships of doping concentration between the lifetime of energy donor/acceptor and phosphorescence energy transfer efficiency; (H) the relationships of doping concentration between the quantum yield of energy donor/acceptor and phosphorescence energy transfer efficiency; (I) luminescence photographs of RB-codoped film TPA-2Py@PVA under and after removing UV irradiation (365 nm) for different duration times.

These pyridine-substituted TPA derivatives with ultralong green-color RTP can be served as energy donors to endow organic fluorescent dyes with longer-wavelength persistent luminescence via the strategy of phosphorescence resonance energy transfer (PRET).

According to the principle of Förster resonance energy transfer (FRET), a good overlap between the emission band of energy donor and the absorption band of energy acceptor is essential for an efficient FRET process. As shown in **Figure 5A,** the absorption band of rhodamine B (RB) overlaps quite well with the RTP emission band of doping film TPA-2Py@PVA, which indicates that an efficient PRET process can be occurred between them to achieve color-tunable persistent luminescence. Indeed, with increasing the doping weight concentration of RB from 1% to 25%, the fluorescence intensity of energy acceptor RB gradually enhances along with the decreased fluorescence intensity of energy donor TPA-2Py (**Figure 5B)**. After delaying 10 ms, the RTP intensity of energy donor TPA-2Py decreases significantly while the fluorescence emission of energy acceptor RB is still retained and further enhanced (**Figure 5C)**. Consequently, we believe that the delayed fluorescence of RB should be derived from the efficient PRET process between the energy donor and acceptor. As far as we know, the FRET will cause a decrease in the excited lifetime of energy donor. As illustrated in **Figure 5D**, the RTP lifetime of energy donor TPA-2Py is indeed decreasing gradually from 718.7 ms to 195.3 ms, confirming the occurrence of PRET between the energy donor and acceptor. On the other hand, the excitation-dependent delayed emission spectra were collected to further confirm the the occurrence of PRET process. As shown in **Figure 5F**, the delayed fluorescence of RB can only be detected by exciting the doping film RB/TPA-2Py@PVA with $\lambda_{ex}$ = 365 nm (the optimal $\lambda_{ex}$ of energy donor TPA-2Py), which indicates that the persistent fluorescence of energy acceptor RB can only be activated via PRET in the presence of energy donor TPA-2Py. According to the principle of FRET, the energy transfer efficiency can be calculated by measuring the lifetime of energy donor in the presence ($\tau_{DA}$) and absence ($\tau_D$) of energy acceptor, respectively.[22] Upon gradually increasing the doping weight concentration of RB from 1% to 25%, the PRET efficiency is remarkably enhanced from 10.0% to 75.5% (**Table S1**). Meanwhile, the delayed fluorescence lifetime of energy acceptor is gradually decreased with increasing PRET efficiency whereas its quantum yield is significantly increased (**Figure 5G-H**). Accordingly, the optimal delayed fluorescence property ($\Phi_P/\tau_P$ = 36.9%/201.6 ms) of energy acceptor RB is obtained at the doping weight concentration of 10%. Besides, multicolor afterglow ranging from green to red can be obtained by simply regulating the doping weight concentration of energy acceptor RB, agreeing well with gradually increased PRET efficiency (**Figure 5I**). The current study demonstrates that PRET is an effective strategy for the achievement of color-tunable organic afterglow by simply assembling the energy donor and acceptor into the polymer matrix.

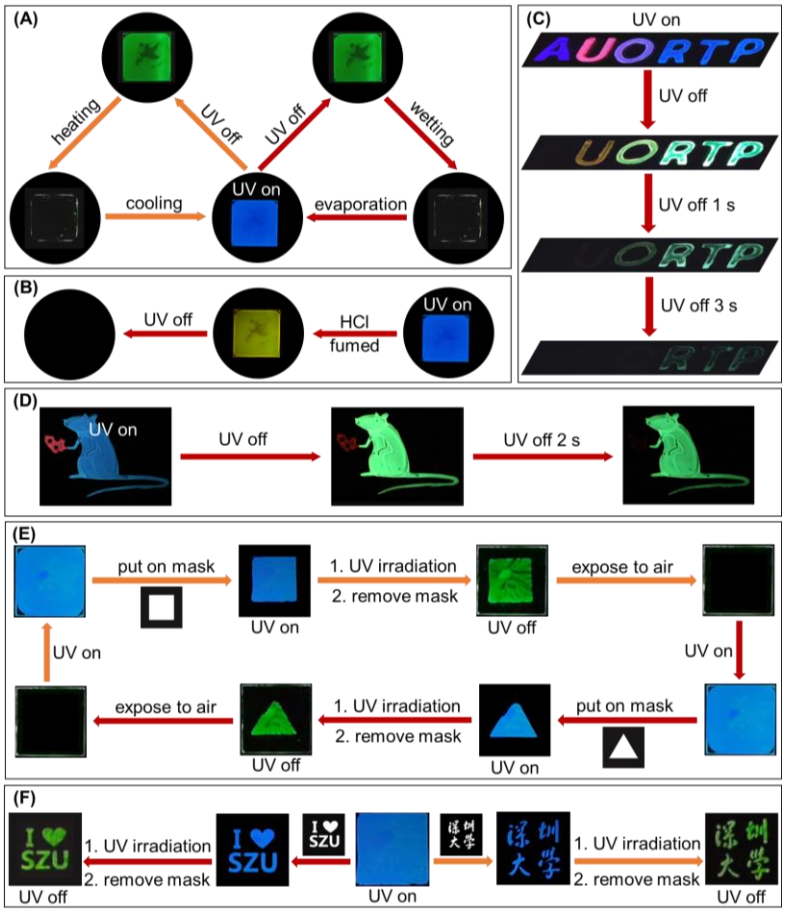


**Figure 6.** Potential applications of doping PVA and PMMA systems in the fields of anti-counterfeiting and information encryption: (A) reversible temperature/humidity-responsive RTP of TPA-2Py@PVA; (B) acid-responsive RTP of TPA-2Py@PVA; (C) time-dependent multicolor RTP based on the word "AUORTP" composing of TPA-2Ph@PVA (A), 15%RhB/TPA-2Py@PVA (U), 5%RhB/TPA-2Py@PVA (O), and TPA-2Py@PVA (RTP), respectively; (D) the pattern "the mouse holding the cheese" is composed of 15%RhB/TPA-2Py@PVA (cheese) and TPA-2Py@PVA (mouse), respectively; (E-F) reversible UV irradiation-responsive RTP of TPA-3Py@PMMA based on various photomasks.

Based on the tunable organic afterglow and UV irradiation-responsive ultralong RTP characteristics of doping PVA and PMMA systems, diverse encryption patterns were prepared to demonstrate their potential applications in advanced anti-counterfeiting and information encryption. It is well known that the RTP property of doping PVA systems is sensitive to water and temperature. As shown in **Figure 6A**, the green afterglow of doping PVA film can be quenched by heating or wetting, and it can then be reactivated by cooling or water evaporation. Considering that the pyridine group is basic, these guest phosphors should respond to the acid stimulation. Indeed, by fuming the doping film TPA-2Py@PVA with concentrated hydrochloric acid, the blue fluorescence is turned into yellow color and the

green afterglow is fully quenched as well (**Figure 6B**). Except for the external stimuli, the multicolor afterglow of RB-codoped PVA film can be used directly. As illustrated in **Figure 6C**, under UV irradiation, the word "AUORTP" composed of four encoding materials with distinct afterglow lifetimes can emit multicolor fluorescence. After ceasing UV irradiation, a new word "UORTP" with multicolor afterglow is observed by the naked eye due to the immediately disappearing letter "A". As time goes by, the letters "U" and "O" with a shorter lifetime fade away successively. Ultimately, the original word "AUORTP" turns into the new word "RTP". In addition, complicated encryption patterns such as a mouse holding a piece of cheese are also designed (**Figure 6D**). Under UV irradiation, what we see is a blue mouse holding a piece of magenta cheese. After removing UV irradiation for different duration times, this pattern is changed into a green mouse holding a piece of red cheese and a green mouse losing its cheese successively. More importantly, advanced information encryption and decryption could be realized by making use of UV irradiation-responsive RTP properties of doping PMMA systems. As shown in **Figure 6E**, by putting a photomask with a square pattern on the film surface, the blue square is turned green after continuous UV irradiation. Then, this green square can be completely erased within 5 min after exposing to the air atmosphere. Subsequently, based on the reversible response characteristics of doping PMMA systems, photomasks with varied patterns such as triangles, Chinese characters of Shenzhen University (SZU), or I♥SZU are designed to demonstrate a new round of information encryption and decryption cycle (**Figure 6F**). These preliminary results demonstrate that pyridine-substituted TPA derivatives studied in this work have great potential applications in advanced anti-counterfeiting and information encryption technologies.

## 3. Conclusion

In summary, we have developed a series of amorphous organic RTP materials with ultralong lifetimes, tunable afterglow, and UV irradiation responsiveness by simply doping pyridine-substituted TPA derivatives as guest phosphors into the PVA and PMMA matrices. On one hand, bright green afterglow lasting for seconds can be observed by the naked eye after embedding these guest phosphors into the PVA matrix, among which doping film TPA-2Py@PVA exhibits the best RTP property with an ultralong lifetime of 798.4 ms and a high phosphorescence quantum yield of 15.2%. Experimental and theoretical studies show that the pyridine group with capabilities of promoting ISC and forming H-bonding interactions with the PVA matrix should be responsible for the achievement of efficient and ultralong RTP of doping PVA systems. On the other hand, no obvious afterglow can be observed by the naked eye after doping these guest phosphors into the PMMA matrix. However, bright green

afterglow is activated under continuous UV irradiation for a few seconds, indicating the photo-activated RTP properties of doping PMMA systems. Experimental results indicate that the UV irradiation-responsive RTP properties of doping PMMA systems can be attributed to the consumption of triplet oxygen after sustaining UV irradiation. Accordingly, these photo-activated RTP emissions will be spontaneously quenched within 5 min after exposure to the air environment. Besides, these doping PVA and PMMA systems with multicolor afterglow and UV irradiation-responsive RTP properties show great application prospects in multilevel anti-counterfeiting and information encryption technologies. We believe that the development of multifunctional polymer-based RTP materials will provide new opportunities for high-tech applications.

**Acknowledgments**

This work was financially supported by the Guangdong Basic and Applied Basic Research Foundation (2023A1515011004), the National Natural Science Foundation of China (21805233, 52273197), the Science and Technology Plan of Shenzhen (JCYJ20180306174910791, KQTD20210811090142053), and Shenzhen Key Laboratory of Functional Aggregate Materials (ZDSYS20211021111400001). The authors also acknowledge the Instrumental Analysis Center of Shenzhen University.

**References**

[1] a) Y. Su, S. Z. F. Phua, Y. Li, X. Zhou, D. Jana, G. Liu, W. Q. Lim, W. K. Ong, C. Yang, Y. Zhao, *Sci. Adv.* **2018**, *4*, eaas9732; b) H. Peng, G. Xie, Y. Cao, L. Zhang, X. Yan, X. Zhang, S. Miao, Y. Tao, H. Li, C. Zheng, W. Huang, R. Chen, *Sci. Adv.* **2022**, *8*, eabk2925; c) X. Dou, T. Zhu, Z. Wang, W. Sun, Y. Lai, K. Sui, Y. Tan, Y. Zhang, W. Z. Yuan, *Adv. Mater.* **2020**, *32*, 2004768.

[2] a) G. Zhang, G. M. Palmer, M. W. Dewhirst, C. L. Fraser, *Nat. Mater.* **2009**, *8*, 747-751; b) X. Zhen, Y. Tao, Z. An, P. Chen, C. Xu, R. Chen, W. Huang, K. Pu, *Adv. Mater.* **2017**, *29*, 1606665; c) W. L. Zhou, W. J. Lin, Y. Chen, Y. Liu, *Chem. Sci.* **2022**, *13*, 7976-7989; d) L. Xu, K. Zhou, H. Ma, A. Lv, D. Pei, G. Li, Y. Zhang, Z. An, A. Li, G. He, *ACS Appl. Mater. Interfaces.* **2020**, *12*, 18385-18394; e) X. F. Wang, H. Xiao, P. Z. Chen, Q. Z. Yang, B. Chen, C. H. Tung, Y. Z. Chen, L. Z. Wu, *J. Am. Chem. Soc.* **2019**, *141*, 5045-5050.

[3] a) A. Fermi, G. Bergamini, M. Roy, M. Gingras, P. Ceroni, *J. Am. Chem. Soc.* **2014**, *136*, 6395-6400; b) Y. Zhou, W. Qin, C. Du, H. Gao, F. Zhu, G. Liang, *Angew. Chem. Int. Ed.*

**2019**, *58*, 12102-12106; c) D. Lee, J. Jung, D. Bilby, M. S. Kwon, J. Yun, J. Kim, *ACS Appl. Mater. Interfaces.* **2015**, *7*, 2993-2997.

[4] a) R. Kabe, N. Notsuka, K. Yoshida, C. Adachi, *Adv. Mater.* **2016**, *28*, 655; b) T. Wang, X. Su, X. Zhang, X. Nie, L. Huang, X. Zhang, X. Sun, Y. Luo, G. Zhang, *Adv. Mater.* **2019**, *31*, 1904273; c) D. R. Lee, K. H. Lee, W. Shao, C. L. Kim, J. Kim, J. Y. Lee, *Chem. Mater.* **2020**, *32*, 2583-2592.

[5] a) W. Zhao, Z. He, J. W. Y. Lam, Q. Peng, H. Ma, Z. Shuai, G. Bai, J. Hao, B. Z. Tang, *Chem.* **2016**, *1*, 592-602; b) S. Zheng, T. Zhu, Y. Wang, T. Yang, W. Z. Yuan, *Angew. Chem. Int. Ed.* **2020**, *59*, 10018-10022.

[6] a) J. Yang, X. Zhen, B. Wang, X. M. Gao, Z. C. Ren, J. Q. Wang, Y. J. Xie, J. R. Li, Q. Peng, K. Y. Pu, Z. Li, *Na. Commun.* **2018**, *9*, 840; b) E. Lucenti, A. Forni, C. Botta, L. Carlucci, C. Giannini, D. Marinotto, A. Pavanello, A. Previtali, S. Righetto, E. Cariati, *Angew. Chem. Int. Ed.* **2017**, *56*, 16302-16307; c) E. Hamzehpoor, D. F. Perepichka, *Angew. Chem. Int. Ed.* **2020**, *59*, 9977-9981.

[7] a) S. Sarkar, H. P. Hendrickson, D. Lee, F. DeVine, J. Jung, E. Geva, J. Kim, B. D. Dunietz, *J. Phys. Chem. C.* **2017**, *121*, 3771-3777; b) S. Cai, H. Shi, D. Tian, H. Ma, Z. Cheng, Q. Wu, M. Gu, L. Huang, Z. An, Q. Peng, W. Huang, *Adv. Funct.Mater.* **2018**, *28, 1705045*.

[8] a) W. Z. Yuan, X. Y. Shen, H. Zhao, J. W. Y. Lam, L. Tang, P. Lu, C. Wang, Y. Liu, Z. Wang, Q. Zheng, J. Z. Sun, Y. Ma, B. Z. Tang, *J. Phys. Chem. C.* **2010**, *114*, 6090-6099; b) O. Bolton, K. Lee, H. J. Kim, K. Y. Lin, J. Kim, *Nat. Chem.* **2011**, *3*, 205-210.

[9] Z. An, C. Zheng, Y. Tao, R. Chen, H. Shi, T. Chen, Z. Wang, H. Li, R. Deng, X. Liu, W. Huang, *Nat. Mater.* **2015**, *14*, 685-690.

[10] a) D. Lee, O. Bolton, B. C. Kim, J. H. Youk, S. Takayama, J. Kim, *J. Am. Chem. Soc.* **2013**, *135*, 6325-6329; b) M. S. Kwon, D. Lee, S. Seo, J. Jung, J. Kim, *Angew. Chem. Int. Ed.* **2014**, *53*, 11177-11181.

[11] a) J. Wang, Z. Huang, X. Ma, H. Tian, *Angew. Chem. Int. Ed.* **2020**, *59*, 9928-9933; b) Z. Y. Zhang, Y. Liu, *Chem. Sci.* **2019**, *10*, 7773-7778.

[12] a) L. Z. J. A. Li, C. Wu, Z. Huang, S. Li, H. Zhang, Q. Yang, Z. Mao, S. Luo, C. Liu, G. Shi, B. Xu, *Angew. Chem. Int. Ed.* **2022**, *62*, e202217284; b) L. Gu, H. Wu, H. Ma, W. Ye, W. Jia, H. Wang, H. Chen, N. Zhang, D. Wang, C. Qian, Z. An, W. Huang, Y. Zhao, *Nat. Commun.* **2020**, *11*, 944; c) R. Tian, S.M. Xu, Q. Xu, C. Lu, *Sci. Adv.* **2020**, *6*, eaaz6107.

[13] a) W. Zhao, Z. He, B. Z. Tang, *Nat. Rev. Mater.* **2020**, *5*, 869-885; b) Kenry, C. Chen, B. Liu, *Nat. Commun.* **2019**, *10*, 2111; c) S. Cai, X. Yao, H. Ma, H. Shi, Z. An, *Aggregate*

**2023**, doi:10.1002/agt2.320.

[14] a) H. Gao, X. Ma, *Aggregate* **2021**, *2*, e38; b) Y. Gong, J. Yang, M. Fang, Z. Li, *Cell Rep. Phys. Sci.* **2022**, *3*, 100663.

[15] a) X. Ma, C. Xu, J. Wang, H. Tian, *Angew. Chem. Int. Ed.* **2018**, *57*, 10854-10858; b) X. Zhang, M. Zeng, Y. Zhang, C. Zhang, Z. Gao, F. He, X. Xue, H. Li, P. Li, G. Xie, H. Li, X. Zhang, N. Guo, H. Cheng, A. Luo, W. Zhao, Y. Zhang, Y. Tao, R. Chen, W. Huang, *Nat. Commun.* **2023**, *14*, 475.

[16] a) M. S. Kwon, Y. Yu, C. Coburn, A. W. Phillips, K. Chung, A. Shanker, J. Jung, G. Kim, K. Pipe, S. R. Forrest, J. H. Youk, J. Gierschner, J. Kim, *Nat. Commun.* **2015**, *6*, 9; b) H. Wu, D. Wang, Z. Zhao, D. Wang, Y. Xiong, B. Z. Tang, *Adv. Funct. Mater.* **2021**, 2101656; c) Z. A. Yan, X. Lin, S. Sun, X. Ma, H. Tian, *Angew. Chem. Int. Ed.* **202**1, *60*, 19735-19739.

[17] a) S. Cai, H. Ma, H. Shi, H. Wang, X. Wang, L. Xiao, W. Ye, K. Huang, X. Cao, N. Gan, C. Ma, M. Gu, L. Song, H. Xu, Y. Tao, C. Zhang, W. Yao, Z. An, W. Huang, *Nat. Commun.* **2019**, *10*, 4247; b) K. Kanosue, S. Ando, *ACS Macro. Lett.* **2016**, *5*, 1301-1305; c) X. Dou, T. Zhu, Z. Wang, W. Sun, Y. Lai, K. Sui, Y. Tan, Y. Zhang, W. Z. Yuan, *Adv. Mater.* **2020**, *32*, 2004768; d) Y. Ren, W. Dai, S. Guo, L. Dong, S. Huang, J. Shi, B. Tong, N. Hao, L. Li, Z. Cai, Y. Dong, *J. Am. Chem. Soc.* **2022**, *144*, 1361-1369.

[18] a) M. Fang, J. Yang, Z. Li, *Acc. Mater. Res.* **2021**, *2*, 644-654; b) Y. Shen, Z. An, H. Liu, B. Yang, Y. Zhang, *Angew. Chem. Int. Ed.* **2023**, *62*, e202214483.

[19] H. Wang, H. Shi, W. Ye, X. Yao, Q. Wang, C. Dong, W. Jia, H. Ma, S. Cai, K. Huang, L. Fu, Y. Zhang, J. Zhi, L. Gu, Y. Zhao, Z. An, W. Huang, *Angew. Chem. Int. Ed.* **2019**, *58*, 18776-18782.

[20] D. Li, J. Yang, M. Fang, B. Z. Tang, Z. Li, *Sci. Adv.* **2022**, *8*, eabl8392.

[21] X. Lin, J. Wang, B. Ding, X. Ma, H. Tian, *Angew. Chem. Int. Ed.* **2021**, *60*, 3459-3463.

[22] S. Kuila, S. J. George, *Angew. Chem. Int. Ed.* **2020**, *59*, 9393-9397.

[23] L. Ma, S. Sun, B. Ding, X. Ma, H. Tian, *Adv. Funct. Mater.* **2021**, *31*, 2010659.

[24] Y. Zhang, L. Gao, X. Zheng, Z. Wang, C. Yang, H. Tang, L. Qu, Y. Li, Y. Zhao, *Na. Commun.* **2021**, *12*, 2297.

[25] a) L. Huang, B. Chen, X. Zhang, C. O. Trindle, F. Liao, Y. Wang, H. Miao, Y. Luo, G. Zhang, *Angew. Chem. Int. Ed.* **2018**, *57*, 16046-16050; b) X. Zhang, L. Du, W. Zhao, Z. Zhao, Y. Xiong, X. He, P. F. Gao, P. Alam, C. Wang, Z. Li, J. Leng, J. Liu, C. Zhou, J. W. Y. Lam, D. L. Phillips, G. Zhang, B. Z. Tang, *Nat. Commun.* **2019**, *10*, 5161; c) J. Ren, Y. Wang, Y. Tian, Z. Liu, X. Xiao, J. Yang, M. Fang, Z. Li, *Angew. Chem. Int. Ed.* **2021**, *60*,

12335-12340; d) X. W. Liu, W. Zhao, Y. Wu, Z. Meng, Z. He, X. Qi, Y. Ren, Z. Q. Yu, B. Z. Tang, *Nat. Commun.* **2022**, *13*, 3887.

[26] a) D. Wang, H. Wu, J. Gong, Y. Xiong, Q. Wu, Z. Zhao, L. Wang, D, Wang, B. Z. Tang, *Mater. Horiz.* **2022**, *9*, 1081; b) D. Wang, J. Gong, Y. Xiong, H. Wu, Z. Zhao, D. Wang, B. Z. Tang, *Adv. Funct. Mater.* **2022**, *33*, 2208895.

[27] a) Y. Wang, J. Yang, M. Fang, Y. Gong, J. Ren, L. Tu, B. Z. Tang, Z. Li, *Adv. Funct. Mater.* **2021**, *31*, 2101719; b) Z. Wang, Y. Zheng, Y. Su, L. Gao, Y. Zhu, J. Xia, Y. Zhang, C. Wang, X. Zheng, Y. Zhao, C. Yang, Y. Li, *Sci. China Mater.* **2021**, *65*, 2160-2168.

[28] M. C. DeRosa, R. J. Crutchley, *Coord. Chem. Rev.* **2002**, *233-234*, 351-371.

**Table of Contents**

we have developed a series of amorphous organic RTP materials with ultralong lifetimes, tunable afterglow, and UV irradiation responsiveness by simply doping pyridine-substituted TPA derivatives into the PVA and PMMA matrices. Diversified encryption patterns are fabricated to demonstrate the potential applications of these doping PVA and PMMA films in multilevel anti-counterfeiting and information encryption technologies.

Shengde Xiong, Yu Xiong*, Deliang Wang, Yiwen Pan, Keyao Chen, Zheng Zhao, Dong Wang, and Ben Zhong Tang*

**Achieving Tunable Organic Afterglow and UV Irradiation-Responsive Ultralong Room-Temperature Phosphorescence from Pyridine-Substituted Triphenylamine Derivatives**